Acta Crystallographica Section A
Foundations of Crystallography
ISSN 0108-7673

Received 8 December 2003
Accepted 7 July 2004

Interlacing of growth steps on crystal surfaces as a consequence of crystallographic symmetry

W. J. P. van Enckevort* and P. Bennema

RIM Department of Solid State Chemistry, Faculty of Science, University of Nijmegen, Toernooiveld, 6525 ED Nijmegen, The Netherlands. Correspondence e-mail: wvenck@sci.kun.nl

During crystal growth, concentric steps of unit-layer thickness [$= d_{(hkl)_u}$, with the surface's *hkl* Miller indices corrected according to the selection rules for non-primitive lattices] are often found to split into lower steps in a regular fashion [Frank (1951). *Phil. Mag.* **42**, 1014–1021]. These 'interlaced' step patterns are introduced by a stacking of two or more growth layers, with different lateral anisotropy in step velocity within each unit layer. In this paper, a general relation between the symmetry of the crystal surface and the configuration of the concentric step patterns thereon is derived and is used to give theoretical shapes of spirals, growth hillocks and etch pits. It is shown that many of the interlaced patterns and their details are imposed by the presence of screw axes and/or glide planes perpendicular to the crystal surface. Finally, the results are compared with the patterns of unit-layer height and lower steps observed by optical and atomic force microscopy on crystals such as SiC, GaN, potash alum, garnet and $NiSO_4{\cdot}6H_2O$.

1. Introduction

In an early paper on the observation of growth spirals on (0001) SiC-6*H*, Verma (1951) reported the occurrence of hexagonal spirals, at the corners of which the unit-cell-height steps split up into steps of half height. These interlaced patterns were interpreted by Frank (1951) as being the result of a periodic stacking of differently oriented growth layers, each having a different lateral anisotropy of step velocity. Later, interlaced step patterns were observed on several other crystal surfaces examined by optical and atomic force microscopy (AFM). Examples are (001) potash alum (van Enckevort *et al.*, 1981), (0001) SiC-4*H* (Sunagawa & Bennema, 1982), (0001) SiC-6*H* (van der Hoek *et al.*, 1982), $(000\bar{1})$ GaN (Nowak *et al.*, 1999; Zauner *et al.*, 2002), (001) $NiSO_4{\cdot}6H_2O$ (van Enckevort & Klapper, 1987), (110) garnet (Bennema *et al.*, 1983, and references therein), (010) acetaminophen (Li *et al.*, 2000) and several proteins (Plomp *et al.*, 2002; Aquilano *et al.*, 2003). The explanations given for these patterns were similar to that given by Frank (1951).

The basic principle of the step interlacing phenomenon is demonstrated by the example given in Fig. 1, which shows a crystal surface, the growth of which proceeds by a successive generation and lateral spreading of two different kinds of layers, of height $d_{hkl}/2$, from a central point, O. Layers of type I are bounded by steps *A* and *B*, whereas the type II layers grow *via* steps *C* and *D*. It is assumed that steps *A* and *D* move quickly, whereas steps *B* and *C* advance slowly. This implies that the fast *A* steps of layer I will catch up with the slow *C* steps of layer II, forming a double-height step of unit height, d_{hkl}. The same happens for the fast steps *D* and the slow steps *B*. This process leads to a pattern consisting of unit-height steps with interlaced crossovers formed by lower steps of height $d_{hkl}/2$. This concept of step interlacing has been encountered in several variations on crystal surfaces examined by phase-sensitive optical microscopy and atomic force microscopy.

Although in a number of papers (van Enckevort *et al.*, 1981, 1993; Bennema *et al.*, 1983; Plomp *et al.*, 2002; Aquilano *et al.*, 2003) a connection has been made between the occurrence of interlacing and the presence of a screw axis or a glide plane perpendicular to the growth surface, no generalized theoretical study of the relationship between step interlacing and crystallographic symmetry has been carried out yet. Three aspects of crystal growth need to be considered: (i) crystallographic symmetry, (ii) the thickness of the growth layers on an *F* face as formulated in the periodic bond chain (PBC; nowadays called connected net) theory for crystal morphology (Hartman & Perdok, 1955*a*,*b*,*c*; Bennema, 1993) and (iii) the anisotropic kinetics of step propagation. Aspect (iii) is specific for the crystal growth situation considered and allows for little generalization. However, by using crystallographic symmetry and a number of basic conclusions derived from the connected net theory, important rules for the occurrence and the characteristics of the various kinds of step interlacing can be derived. In the present paper, it will be shown that in many cases interlacing is imposed by symmetry and 'must' occur; this situation will be called '*symmetry-induced interlacing*'. In a few cases, interlacing not imposed by symmetry may occur, which we denote as '*incidental interlacing*'. The characteristics of both types, with emphasis on the symmetry-induced interlacing, and rules for their occurrence will be derived. The

theoretical results will be compared with observations reported in the literature.

2. Incidental and symmetry-induced interlacing: some basic properties

2.1. Integrated connected net theory and roughening transition theory

The occurrence of interlacing implies the presence of growth steps on the crystal surface. The physical basis for the occurrence of growth steps is given by the connected net theory integrated with the theory of roughening transition. The original Hartman–Perdok theory (Hartman & Perdok, 1955*a*,*b*,*c*; Hartman, 1973, 1987) forms the basis of the modern connected net theory (Bennema, 1993). The integration of this morphological theory with the concept of roughening transition was carried out by Rijpkema *et al.* (1983) and Bennema (1993, 1996). For recent developments in this theory, the reader is referred to Grimbergen *et al.* (1998, 1999), Meekes *et al.* (1998) and Bennema *et al.* (2003).

In order to derive the morphology of crystals and to verify whether steps can occur on a given crystal surface, according to the above-mentioned theory, the 'crystal graph' of the crystal under investigation has to be partitioned into connected nets. The procedure to find connected nets can be summarized as follows (Bennema, 1993). First, the 'crystal graph' corresponding to the crystal structure has to be determined. A 'crystal graph' is a construction composed of the centres of gravity of the growth units (atoms, molecules or ions) from which the crystal was growing and the (generally first nearest neighbour) bonds between the growth units. Then the occurrence of one or more connected networks of growth units is searched for orientations (*hkl*). Such a connected net must be confined to within a slice of overall thickness d_{nhnknl}, as defined by the BFDH (Bravais, Friedel, Donnay and Harker) law. According to this law, d_{hkl} is the interplanar distance between adjacent planes with Miller indices *hkl*. Because of the selection rules of the space group introduced by a non-primitive lattice, screw axes or glide planes, the interplanar distance may be reduced. The slice thickness then becomes d_{nhnknl}, with n = 1, 2, 3, 4, 6. The BFDH law states that the higher the value of d_{nhnknl} the more often and/or larger the face (*hkl*) that is expected to appear on the equilibrium and growth form of the crystal.

If it is possible to partition the crystal graph into parallel connected nets that fit within the slice thickness as defined in the BFDH law then it can be shown that a surface with orientation (*hkl*) parallel to such a connected net will have a roughening temperature larger than 0 K. For such a surface, normally denoted as an '*F* face', the step free energy is positive for all crystallographic directions coplanar with (*hkl*). If such a face is growing below its roughening temperature, then it will grow as a flat face with a step mechanism.

This paper will concentrate on those *F* faces (*hkl*) for which two or more (not translation-equivalent) connected nets are stacked upon each other within one interplanar distance d_{hkl}. If the nets are not roughened, interlaced step patterns may develop on such faces.

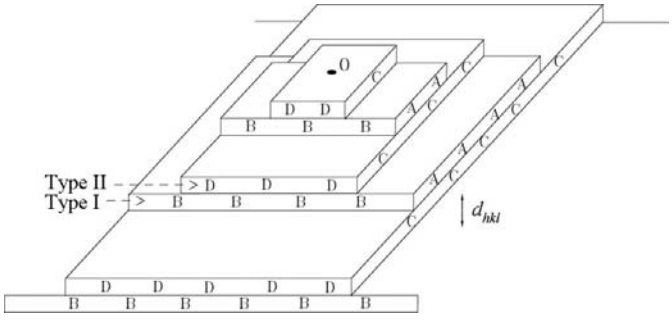

Figure 1
An example demonstrating the principle of step interlacing, viewed in perspective. Closed-loop steps are periodically generated at the hillock centre O. At the corners of the growth patterns, the unit-height steps *CA* and *BD* split into half-unit-height steps *B* and *C*.

2.2. Conditions, mechanism and shape of step interlacing

Adjacent slices d_{hkl}, with Miller indices *hkl* corrected for the systematic extinctions of non-primitive lattices, are translation equivalent and must generate identical step patterns on an *F* surface parallel to plane (*hkl*). In the following, these slices will be referred to as slices with unit thickness $d_{(hkl)_u}$ or, briefly, unit slices. For example, the unit slice parallel to the (110) face in a *P* lattice has thickness d_{110}, in an *F* lattice d_{220} and in an *A* lattice d_{220}. If the thickness of the connected net is equal to $d_{(hkl)_u}$, the minimum step height is also $d_{(hkl)_u}$ and no splitting into lower steps, *i.e.* no interlacing, will occur.

However, if $d_{(hkl)_u}$ consists of a sequential stacking of two or more connected nets then a splitting up of unit-height steps into lower steps may take place. In this case, the different, connected, subslices generate growth steps, each with a different lateral anisotropy of propagation velocity. Because of these differences in velocity, the fast substeps overtake the slower ones and recombination to new unit-height steps occurs, as shown in Fig. 2(*a*). For each direction, the bottom subslice of the unit steps is the slowest advancing step in that direction. If for a changing orientation of the unit step the identity of the slowest, and thus the lowest, substep changes, the height difference introduced must be compensated by a splitting off and a subsequent recombination of one or more substeps (Fig. 2*b*). This is the basic principle of step interlacing.

If one considers a series of closed-loop steps of subunit height emitted from a central source then in each period $d_{(hkl)_u}/R$ (R is the growth rate of the crystal) a sequence of substeps with total height $d_{(hkl)_u}$ is generated. For each set within $d_{(hkl)_u}$, the faster moving steps will catch up with the slowest moving one and an equidistant step train of unit-height steps will develop. For each direction θ, the lowest subslice of each unit step corresponds to the slowest substep in that direction. As shown in Fig. 3, the general shape of the closed loop of unit-height steps is identical to the inscribed figure of the anisotropic loop shapes of the substeps if they can

propagate freely. The concentric patterns of 'free' substeps can be derived from the lateral anisotropy of propagation velocity of these steps and by using the 'kinetic Gibbs–Wulff' construction (van Suchtelen, 1995, and references therein) in two dimensions. Step splitting occurs at the points of intersection of the different substep patterns, that is, at sharp corners of the inscribed figure. The rectilinear regions of step splitting that radiate from the centre of the concentric step pattern towards the sharp corners of the unit step pattern will be denoted as '*interlacing trajectories*' in the following. The details of step splitting will be elaborated in §3.

2.3. Impact of symmetry

Two cases for the occurrence of connected subnets can be distinguished. First, the sublayers are not related to one another by symmetry, are related by an inversion point or are related by symmetry elements parallel to the growth surface. For instance, as shown in Fig. 4(*a*), for a twofold axis parallel to the surface, no symmetry relationship exists between the lateral anisotropy of step velocity for the adjacent sublayers.

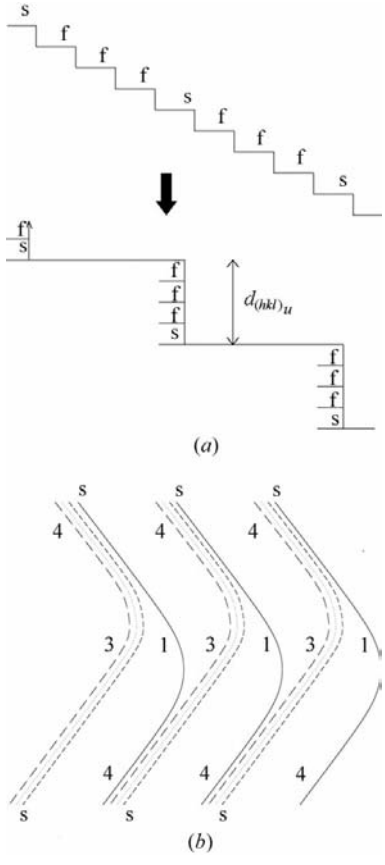

Figure 2
The basics of step interlacing. (*a*) Recombination of a periodic sequence of substeps to a periodic sequence of unit-height steps $d_{(hkl)_u}$. Here the faster substeps (f) catch up with the slowest propagating one (s), and for each unit-height step the bottom slice corresponds to the slowest substep. (*b*) If for a changing orientation of the unit step the identity of the slowest, and thus the lowest, substep changes, the height difference must be compensated by a splitting off and subsequent recombination of one or more substeps.

The interlacing evolving from these situations is not imposed by symmetry and therefore it will be denoted as '*incidental interlacing*' in the following. It is important to realize that in this case the top surfaces of the sublayers are not symmetrically related and thus are essentially different. This difference leads to a different surface free energy for each sublayer and therefore to a different growth rate for each layer. It is to be expected that in many cases the sublayer with the highest surface free energy grows slowest in all directions and no change in the identity of the slowest step occurs. Therefore incidental interlacing is less common and, as far as is known to us, has only been revealed during an *in situ* study of (001) $K_2Cr_2O_7$ etched in a 0.7% water–ethanol mixture (Plomp *et al.*, 2000).

If for an *F*-type surface the splitting up of $d_{(hkl)_u}$ into connected subnets is imposed by symmetry and the anisotropy in step advancement velocity of these sublayers is related by symmetry, then the resulting interlacing of steps will be indicated as '*symmetry-induced interlacing*'. This situation results if a translation less than $d_{(hkl)_u}$ perpendicular to the growth surface $z(x, y)$ occurs in combination with a point symmetry operation that does not change the heights $z(x, y)$ of all surface places. Therefore, the action of a rotation axis or a

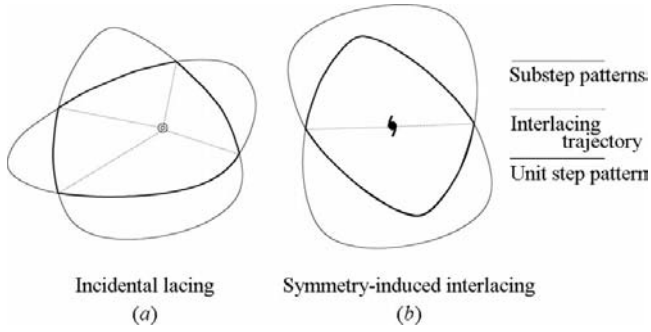

Figure 3
The general shape of the closed loop of unit-height steps is identical to the inscribed figure of the anisotropic shapes of the subunit steps if they can propagate freely: (*a*) incidental interlacing; (*b*) symmetry-induced interlacing imposed by a 2_1 axis.

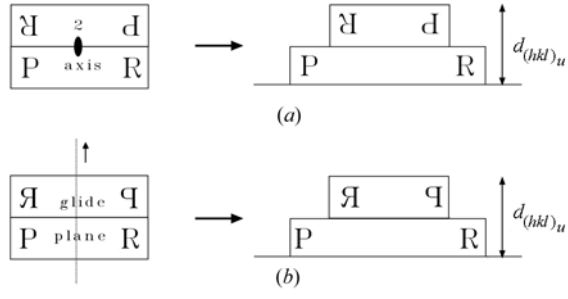

Figure 4
The anisotropic propagation velocity of adjacent substeps is only related by symmetry if a rotation axis or a mirror plane combined with a translation of less than $d_{(hkl)_u}$, both perpendicular to the surface, is present. This combination leads to symmetry-induced interlacing. (*a*) A twofold axis parallel to the surface can give incidental interlacing; (*b*) a glide plane perpendicular to the surface 'must' give symmetry-induced interlacing.

mirror plane perpendicular to the surface together with a translation less than $d_{(hkl)_u}$, also perpendicular to the surface (Fig. 4*b*), is required. In other words, symmetry-induced interlacing is expected if screw axes and/or glide planes perpendicular to the growth surface are present. The translation vector of the glide plane must not be parallel to the surface. The connectedness of the subslices, which is necessary to permit growth *via* steps of subslice height, follows directly from the PBC theory, namely, the above-mentioned faces are only *F* type if a connected net of growth units fits within each subslice of thickness d_{hkl}/n, with $n = N/m$ if $m \leq N/2$, or $n = N/(N - m)$ for an N_m screw axis ($n = 2$ for an *a*-, *b*-, *c*- or *n*-glide plane and $n = 2$ or 4 for a *d*-glide). Of course, d_{hkl}/n must be less than $d_{(hkl)_u}$, and the connected nets should not be thermally or kinetically roughened.

As concluded from the above, symmetry-induced step interlacing occurs during the growth of those *F* faces upon which a perpendicular screw axis and/or a perpendicular glide plane is present. The translation of the glide plane must have a finite component, less than $d_{(hkl)_u}$, normal to the surface. Since such faces show systematic extinction of X-ray reflections, a general rule for the occurrence of symmetry-induced interlacing can now be given. The rule is *if a plane with Miller indices (hkl) corrected for the systematic extinctions of non-primitive lattices and being parallel to a connected net in the crystal exhibits a systematic extinction of X-ray reflection then symmetry-induced interlacing is to be expected on a crystal surface parallel to this plane*. As will be discussed in §4, despite this 'strict' rule, in several cases the interlacing is absent as a consequence of pseudosymmetry.

For both incidental and symmetry-induced interlacing, the macroscopic symmetry of the unit-height step patterns follows Neumann's rule (*e.g.* Nye, 1984) and is determined by the two-dimensional point group of the surface. For incidentally interlaced patterns, the situation is obvious, since the symmetry of each subslice, and thus of the whole stack $d_{(hkl)_u}$, is determined by the point-symmetry elements perpendicular to the surface. Here the symmetry is exact. For the patterns resulting from symmetry-induced interlacing, one has to consider the projection of the step patterns onto the (*hkl*) plane. In this case, the translations perpendicular to $z(x, y)$ 'vanish' and the point-group symmetry resulting from all the symmetry elements perpendicular to this surface remains. For instance, the pattern of unit steps forced by a 2_1 axis, as shown in Fig. 3(*b*), exhibits twofold symmetry. A unit-height pattern generated by an N_m axis shows *n*-fold symmetry, whereas the unit step pattern resulting from a glide plane exhibits mirror symmetry. The number and the orientation of the interlacing trajectories are also subjected to the two-dimensional point-group symmetry of the crystal surface. For a screw axis N_m perpendicular to the surface, the number of interlacing trajectories must be uN [for a 2_1 axis $2 + 4(u - 1)$, as will be elaborated in §3.3], with u a positive integer. For a glide plane perpendicular to the surface, there must be $2 + 2(u - 1)$ interlacing trajectories, the first two being parallel to the glide mirror plane. In §3, it will be shown that in the case of symmetry-induced interlacing the two-dimensional point-group symmetry of the step patterns is approximate rather than exact.

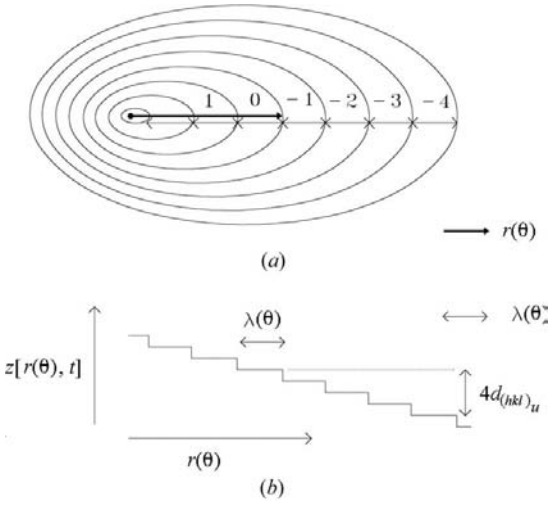

Figure 5
A concentric step pattern emitted from a central source: (*a*) top view; (*b*) side view.

3. Symmetry of concentric interlaced step patterns

3.1. Periodicity

Consider a point source on a crystal surface (*hkl*), which emits 'step sequences' periodically with frequency $f = R/d_{(hkl)_u}$. A 'step sequence' is here defined as a group of adjacent subunit steps, the sum of the heights of which equals one unit-slice thickness, $d_{(hkl)_u}$. The step velocity, $\mathbf{v}_{st}(\theta)$, is defined as the displacement velocity of the steps in the direction parallel to the position vector $\mathbf{r}(\theta)$, which generally is not the direction perpendicular to the step. The origin of the coordinate system $\mathbf{r}(\theta)$ coincides with the centre that emits steps. The velocity $\mathbf{v}_{st}(\theta)$ is assumed to be constant in time. In the first instance, we consider the case $d_{hkl}^{\text{slice}} = d_{(hkl)_u}$, *i.e.* the step height equals the unit-slice thickness $d_{(hkl)_u}$. This situation is shown in Fig. 5. The periodicity of the step pattern in space can now be expressed as

$$z[\mathbf{r}(\theta), t] = z[\mathbf{r}(\theta) + i\boldsymbol{\lambda}(\theta), t] + id_{(hkl)_u}. \quad (1)$$

In this equation, $z[\mathbf{r}(\theta), t]$ is the height of the crystal surface at position $\mathbf{r}(\theta)$ and time t, $\boldsymbol{\lambda}(\theta)$ is the step spacing in direction $\mathbf{r}(\theta)$, which equals $\mathbf{v}_{st}(\theta)/f$, and i is an integer corresponding to the number of steps between $\mathbf{r}(\theta)$ and $\mathbf{r}(\theta) + i\boldsymbol{\lambda}(\theta)$. At a fixed position $\mathbf{r}(\theta)$, the periodicity in time is formulated as

$$z[\mathbf{r}(\theta), t] = z[\mathbf{r}(\theta), t + j/f\,] - jd_{(hkl)_u}, \quad (2)$$

where j is the number of steps that passed $\mathbf{r}(\theta)$ during the time interval j/f.

From the assumption that $z[\mathbf{r}(\theta), t]$ is a pattern of steps generated from a central point, which advance at a constant velocity, it follows that

$$z[\mathbf{r}(\theta), t] = z\{\mathbf{r}(\theta) - t\mathbf{v}_{st}(\theta)\}, \quad (3)$$

with $\mathbf{r}(\theta) - t\mathbf{v}_{st}(\theta) \geq 0$.

Combining (1)–(3) gives the periodicity of a concentric step pattern in space and time:

$$z[\mathbf{r}(\theta), t] = z\{\mathbf{r}(\theta) + i\boldsymbol{\lambda}(\theta) - (t + j/f)\mathbf{v}_{st}(\theta)\} + (i - j)d_{(hkl)_u}, \quad (4)$$

or equivalently $[\boldsymbol{\lambda}(\theta) = \mathbf{v}_{st}(\theta)/f]$

$$z[\mathbf{r}(\theta), t] = z\{\mathbf{r}(\theta) + (i - tf - j)\boldsymbol{\lambda}(\theta)\} + (i - j)d_{(hkl)_u}. \quad (5)$$

In these equations, the integers i and j denote the periodicity in space and time, respectively. For etch pits, one has to take the slice thickness as a negative number, *i.e.* $d_{(hkl)_u} = -|d_{(hkl)_u}|$, because layers are removed.

3.2. Symmetry

In observing crystal surfaces by AFM or by phase-sensitive optical microscopy, surface features reflecting the macroscopic two-dimensional point-group symmetry of the surface can be revealed. However, since these techniques are capable of detecting height differences down to atomic distances, translations perpendicular to the surface can also be imaged. As discussed in §2, both are the effects from all the symmetry elements that are perpendicular to the growth surface. These comprise those symmetry operators O = {M, T} that fulfil

$$z[\mathbf{r}(\theta), t] = z\{\mathrm{M}[\mathbf{r}(\theta)], t\} + \mathrm{T}d_{(hkl)_u}, \quad (6)$$

where M is the transformation matrix and T < 1 is the translation component perpendicular to the surface. In fact, the set of (2 × 2) matrices M describes the macroscopic point-group symmetry of the surface. Examples of O are n-fold axes and mirror planes perpendicular to the surface O = {M, 0}. To have some relevance for the case of symmetry-induced interlacing, it is necessary that 0 < T < 1. This condition occurs for screw axes and glide planes perpendicular to the surface, $\mathrm{O} \cong \{\mathrm{M}, \mathrm{T}\} = \{\mathrm{M}, 1/n\}$. Other symmetry operators, like inversion ($z[\mathbf{r}(\theta), t] = -z\{-[\mathbf{r}(\theta)], t\}$), that do not fulfil the symmetry requirement (6) do not influence the symmetry of the crystal surface as seen by optical microscopy and AFM.

Application of a pure point-symmetry operator, O = {M, 0}, of the above type gives

$$z[\mathbf{r}(\theta), t] = z\{\mathrm{M}[\mathbf{r}(\theta)], t\}, \quad (7)$$

which is merely Neumann's rule. For instance, crystal surfaces with a perpendicular fourfold axis exhibit spirals, hillocks and etch pits with fourfold symmetry. Application of a screw or glide operation, O = {M, T}, of the above type yields in combination with (4) essentially different results:

$$\begin{aligned} z[\mathbf{r}(\theta), t] &= z\{\mathbf{r}(\theta) + i\boldsymbol{\lambda}(\theta) - (t + j/f)\mathbf{v}_{st}(\theta)\} + (i - j)d_{(hkl)_u} \\ &= z\{\mathrm{M}[\mathbf{r}(\theta) + i\boldsymbol{\lambda}(\theta) - (t + j/f - T/f)\mathbf{v}_{st}(\theta)]\} \\ &\quad + (i - j + \mathrm{T})d_{(hkl)_u} \\ &= z\{\mathrm{M}[\mathbf{r}(\theta)], t - \mathrm{T}/f\} + \mathrm{T}d_{(hkl)_u}. \end{aligned} \quad (8)$$

It is clear from the above equation that Neumann's rule, as formulated in (7), is no longer valid. This outcome is explained by the fact that the dimension viewed perpendicular to the surface is no longer macroscopic but is observed on a molecular scale.

An important consequence of (8) is that upon applying symmetry operator O the equivalent position of $z[\mathbf{r}(\theta), t]$ is at $\mathrm{M}[\mathbf{r}(\theta)]$, at $\mathrm{T}d_{(hkl)_u}$ higher and at a time T/f earlier. A time T/f earlier is identical to a shift back over a distance $|\mathbf{v}_{[st}(\theta)\mathrm{T}/f|$ along direction $\mathrm{M}[\mathbf{r}(\theta)]$. Of course, further symmetry-equivalent positions are generated by the translation symmetry in place and time as described by (4) and (5). This information is also included in (8). The underlying physics is that T/f is the time needed to generate a new sublayer at the growth centre before this sublayer is emitted.

As an example, the use of (8) is demonstrated for a twofold screw axis perpendicular to the surface

$$\mathrm{O} = \left\{ \begin{bmatrix} -1 & 0 \\ 0 & -1 \end{bmatrix}, \tfrac{1}{2} \right\}.$$

Equation (8) gives a step pattern that fulfils the symmetry relation

$$\begin{aligned} z[\mathbf{r}(\theta), t] &= z\{\mathbf{r}(\theta) + i\boldsymbol{\lambda}(\theta) - (t + j/f)\mathbf{v}_{st}(\theta)\} + (i - j)d_{(hkl)_u} \\ &= z\{\mathrm{M}[\mathbf{r}(\theta) + i\boldsymbol{\lambda}(\theta) - (t + j/f - 1/2f)\mathbf{v}_{st}(\theta)]\} \\ &\quad + (i - j + 1/2)d_{(hkl)_u} \\ &= z\{-\mathbf{r}(\theta) - i\boldsymbol{\lambda}(\theta) + (t + j/f - 1/2f)\mathbf{v}_{st}(\theta)\} \\ &\quad + (i - j + 1/2)d_{(hkl)_u} \\ &= z[-\mathbf{r}(\theta), t - 1/2f\} + d_{(hkl)_u}/2. \end{aligned} \quad (9)$$

This equation implies that a symmetry-equivalent point $\mathbf{r}(\theta)$ can be found by the successive application of (i) a twofold rotation, (ii) an increase in height of $d_{(hkl)_u}/2$, or (iii) going back in time by $1/2f$, which is identical to a shift back over a distance $|\mathbf{v}_{st}(\theta)/2f| = |\boldsymbol{\lambda}(\theta)/2|$ along direction $-\mathbf{r}(\theta)$. The simplest pattern and a more complex pattern of interlaced steps that fulfil the symmetry given by (9) are shown in Fig. 6.

3.3. Implications and examples

Fig. 7 shows the patterns of symmetry-induced interlacing for the various screw axes and glide planes that can occur perpendicular to a growing F-type surface. Here only the simplest cases are shown: only one single symmetry element perpendicular to the growth surface and the lowest possible number of interlacing trajectories. For a glide plane, the minimum number of trajectories is two; for an N_m screw axis the minimum is N. In deriving the patterns, (8) is used in a fashion similar to that discussed in the previous section for the 2_1 axis. It can clearly be recognized that the characteristics of the interlacing patterns and the step splitting involved are determined by the central symmetry element. The simple interlacing patterns of Fig. 7 are expected to be the most common encountered in experiments.

Including more complicated patterns determined by one single N_m screw axis or one glide plane perpendicular to the surface, (8) can only be fulfilled if the number of trajectories equals uN and $2 + 2(u - 1)$, respectively, with u a positive integer. One exception is the 2_1 screw axis for which the

number of trajectories must be $2 + 4(u - 1)$. This expression follows from the fact that, upon application of (9) to a given surface site, for a 2_1 axis the equivalent point is 1/2 times (plus an integer value, which will not be considered here) higher or lower. Since each trajectory corresponds to a height jump of $+1/2$ or $-1/2$, to reach this position along a given step (route I in Fig. 6*b*) one must pass an odd number of interlacing trajectories. The same holds for the symmetrically equivalent route II back to the original position. Therefore, the total number of interlacing trajectories is twice an odd number, or $2 + 4(u - 1)$. An alternative approach to deducing the number of interlacing trajectories for a 2_1 axis is by considering the number of intersection points of two equivalent step patterns that are rotated 180° with respect to one another. This value also amounts to $2 + 4(u - 1)$ and is, as elaborated in §2.2, identical to the number of interlacing trajectories.

In many cases, a cooperation of different screw axes, glide planes and other symmetry elements perpendicular to the growth face exists, which leads to more or less complex interlacing patterns. For all these symmetry elements the step pattern must obey (7) and (8). An example is given in Fig. 8, which shows a possible interlacing pattern on the (0001) surface of a crystal with space group $P6_3mc$. The interlacing pattern fulfils the symmetry requirements imposed by the 6_3 axis and the three *c*-glide planes according to (8), as well as those imposed by the three mirror planes according to Neumann's rule given by (7).

The presence of a screw axis or glide plane perpendicular to a growth face does not necessarily lead to symmetry-induced interlacing. For several orientations in non-primitive space groups, the subslices that result from the occurrence of screw axes and glide planes are identical to unit slices in these non-primitive lattices. Often in such groups the N_m screw axes are parallel to *n*-fold axes or the glide planes are parallel to mirror planes. Examples of both situations are the (020) slices perpendicular to the 2_1 axes and the (200) slices perpendicular to the *a*-glides in space groups *C*2 and *Cm*, respectively. In these cases, no symmetry-induced interlacing will occur for the

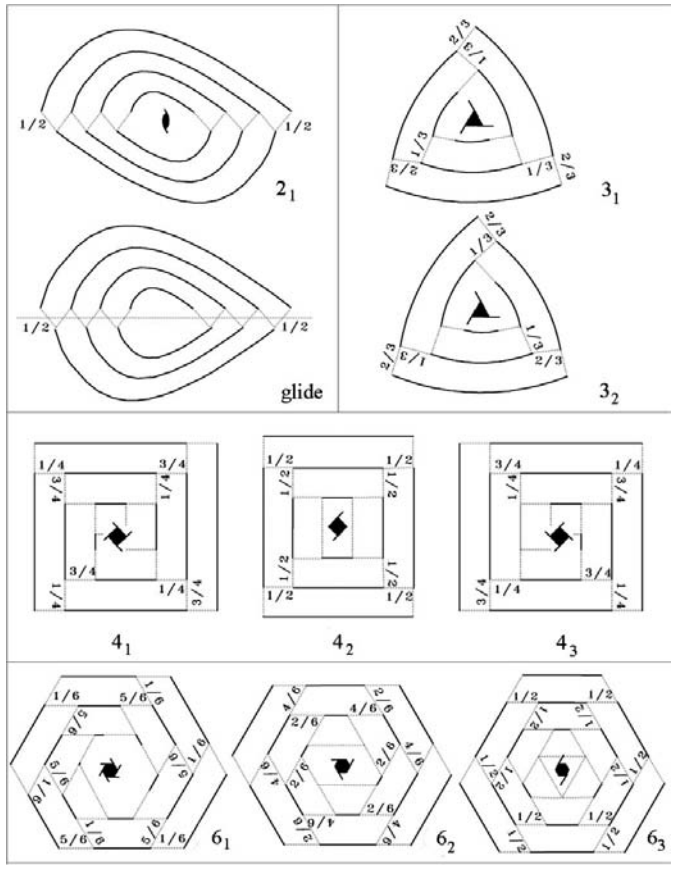

Figure 7
The simplest possible patterns of symmetry-induced interlacing that are imposed by one single screw axis or one glide plane perpendicular to the growing crystal surface. The 6_4 and 6_5 patterns are mirror images of 6_2 and 6_1, respectively.

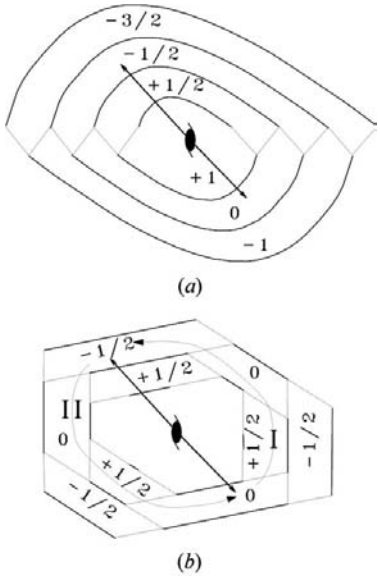

Figure 6
The simplest (*a*) and a more complex (*b*) pattern of symmetry-induced interlacing, which is imposed by a twofold screw axis perpendicular to the growth surface.

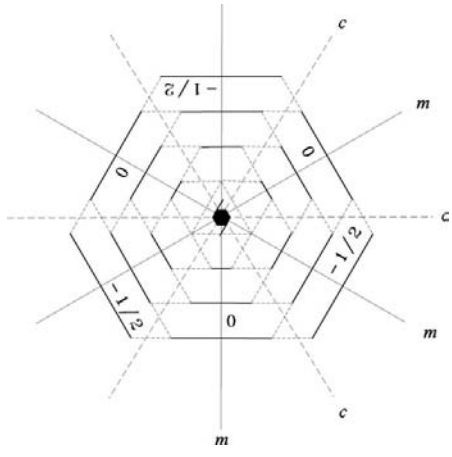

Figure 8
A symmetry-induced interlacing pattern on the (0001) surface of a crystal with space group $P6_3mc$. The symmetry elements perpendicular to the surface are also given.

respective (010) and (100) faces, since the adjacent slices are translation equivalent. Furthermore, in a number of primitive space groups, screw axes and glide planes exist that span two unit slices, $d_{(hkl)_u}$. Again, the slices are translation equivalent and the corresponding surfaces will not show symmetry-induced interlacing. An example is the (110) face of tetragonal lysozyme, which does not reveal interlacing despite the presence of a perpendicular 2_1 axis (Plomp *et al.*, 2002). This circumstance is explained by the fact that in space group $P4_32_12$, in which this protein crystallizes, the 2_1 axis perpendicular to (110) spans two unit slices d_{110}. The above implies that, in considering the relevance of screw axes and glide planes for the occurrence of symmetry-induced interlacing, one has to consider strictly the systematic extinction criterion as formulated in §2.2.

4. Confrontation with some experiments

4.1. Regular patterns

The first case of step interlacing reported in the literature was the hexagonal cross-laced spiral pattern on (0001) SiC-6*H*, as observed by Verma (1951) and interpreted by Frank (1951). The pattern they observed was identical to that drawn in Fig. 8. As discussed in §3.3, this pattern is in accordance with the various symmetry elements perpendicular to the (0001) surface of a crystal structure with space group $P6_3mc$. The same interlacing pattern was also encountered for the (0001) surfaces of other compounds crystallizing in space group $P6_3mc$, such as SiC-4*H* (Sunagawa & Bennema, 1979; van der Hoek *et al.*, 1982) and GaN (Nowak *et al.*, 1999; Zauner *et al.*, 2002).

Interlacing patterns introduced by a single 2_1 axis, in the absence of other symmetry elements perpendicular to the surface, were found on the (010) face of the steroid 7αMNa (space group $P2_1$) for growth (Stoica *et al.*, 2004) and on the (010) face of acetaminophen (space group $P2_1/n$) for etching (Li *et al.*, 2000).

In 1981, the interlacing pattern in Fig. 9 was observed on the (001) surfaces of potash alum [$KAl(SO_4)_2\cdot 12H_2O$] crystals by using optical phase contrast microscopy (van Enckevort *et al.*, 1981). Potash alum crystallizes in space group $P2_1/a\bar{3}$. As follows from a PBC analysis (Hartman, 1969) and from surface topography (van Enckevort *et al.*, 1981), the (001) form grows as an *F* face with slice thickness d_{200}. In superposition on the step pattern, Fig. 9 also gives all the symmetry elements that are perpendicular to the (001) surface. Using (8), it can be shown that the step pattern is identical to the simplest possible interlacing figure that can be obtained by the combined action of the three perpendicular symmetry elements. Here the *c*-glide and the 2_1 axis generate the interlacing pattern. The *b*-glide plane, which has no translation component perpendicular to the (001) surface, induces no interlacing but makes the step pattern mirror symmetric along [010]. On the octahedral surfaces of the potash alum crystals, no interlacing was observed. This result agrees with the fact that in $P2_1/a\bar{3}$ the (*hhh*) planes do not exhibit systematic extinction of X-ray reflections.

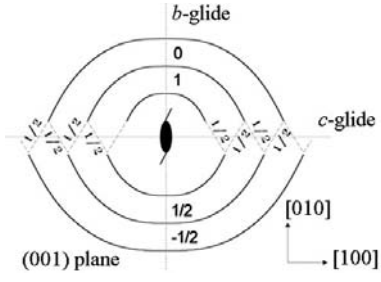

Figure 9
A symmetry-induced interlacing pattern on the (001) surface of a crystal, such as potash alum, that crystallizes in space group $P2_1/a\bar{3}$. The symmetry elements perpendicular to the surface are also given.

Another example of step interlacing that is introduced by a combination of symmetry elements was observed for growth spirals on the (110) surfaces of flux-grown garnet crystals. These interlacing patterns, which were observed with the help of optical phase contrast microscopy by Cherepanova *et al.* (1989), are described in detail by Bennema *et al.* (1983). The patterns are characterized by four perpendicular interlacing trajectories at which unit steps with height d_{110} split into two

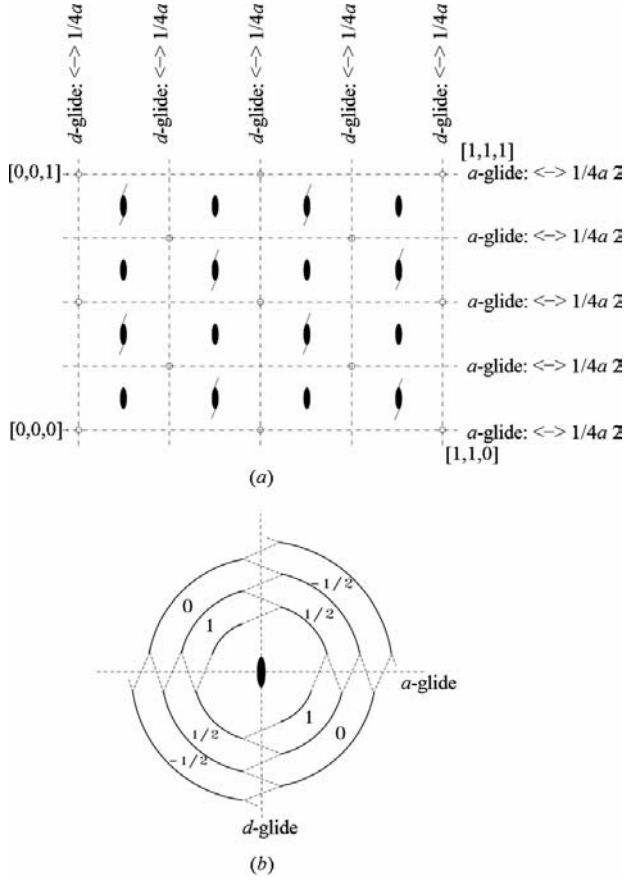

Figure 10
A symmetry-induced interlacing pattern on the $(1\bar{1}0)$ surface of a crystal, such as garnet, that crystallizes in space group $Ia\bar{3}d$. (*a*) Symmetry elements perpendicular to the growth surface plus inversion points; (*b*) the pattern of interlaced steps.

lower steps, d_{220}. The (110) planes are 'forbidden' according to the selection rules of the space group $Ia\bar{3}d$ of garnet but are 'allowed' by its I operator. Therefore, on the (110) surfaces, symmetry-induced interlacing is expected to occur. Following the selection rules of the space group, the thickness of the subslices is d_{220}. Fig. 10(a) shows the symmetry elements perpendicular to the $(\bar{1}10)$ plane in space group $Ia\bar{3}d$. The relevant symmetry elements are the a-glides and the d-glides, both with a translation component d_{220} perpendicular to the surface, and the twofold axes. The 2_1 screw axes involve a translation equal to d_{110}, which is identical to the unit-slice thickness. Therefore, these symmetry elements do not affect the interlacing pattern. With the help of (7) and (8), it can be deduced that the simplest interlacing pattern, which is consistent with the combined action of the three relevant symmetry operators, is that shown in Fig. 10(b). Here the a- and d-glide planes generate the four perpendicular interlacing trajectories and the 2 axis makes the complete figure twofold symmetric. The step pattern of Fig. 10(b) is identical to that observed by optical microscopy. The spirals on the (112) faces of the flux-grown garnet crystals did not reveal interlacing of steps. This observation agrees with the fact that, according to the selection rules of space group $Ia\bar{3}d$, the ($hh2h$) planes are not forbidden.

A final example of growth spirals exhibiting step interlacing was observed on the (001) surfaces of $NiSO_4{\cdot}6H_2O$ crystals, which were grown from an aqueous solution (van Enckevort & Klapper, 1987). The step pattern as observed by optical phase contrast microscopy is schematized in Fig. 11. In this figure, two very broad interlacing trajectories can be recognized, at which the unit-height steps, d_{001}, split into two half-unit-height steps, d_{002}. The space group of $NiSO_4{\cdot}6H_2O$ is $P4_12_12$ (O'Connor & Dale, 1966). In this space group, the symmetry elements perpendicular to the (001) growth surface are the 4_1 and 2_1 axes. The simplest possible interlacing pattern on such a surface is identical to that drawn in Fig. 7 for the case of a single 4_1 axis perpendicular to the growth surface. This pattern is essentially different from the observed features as presented in Fig. 11. The observed interlacing, however, is consistent with the occurrence of only a twofold screw axis perpendicular to the growth surface. This indicates a symmetry lowering from $P4_12_12$ to $P2_12_12$. In other words, judging from the interlaced surface patterns as revealed by optical microscopy, the symmetry of the $NiSO_4{\cdot}6H_2O$ crystals investigated by van Enckevort & Klapper (1987) appears to be orthorhombic rather than tetragonal. A difference in crystallographic symmetry as determined by X-ray diffraction and as deduced from crystal growth properties (hypomorphism) is not uncommon; such a discrepancy has also been encountered for $NH_4H_2PO_4$ (Bennema, 1965; Verheijen *et al.*, 1996), $K_2Cr_2O_7$ (Derksen *et al.*, 1994, and references therein; Heide & Follner, 1996; Heide *et al.*, 1996; Plomp *et al.*, 2000) and $Ba(NO_3)_2$ (Maiwa *et al.*, 1998).

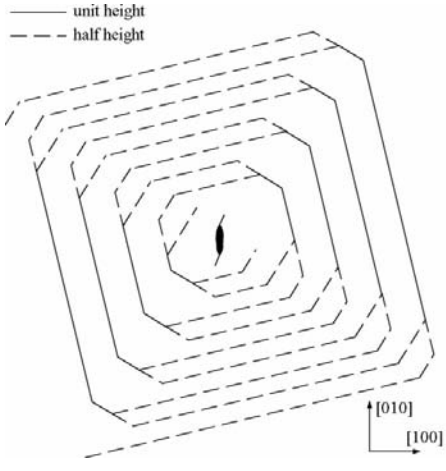

Figure 11
A symmetry-induced interlacing pattern made up of d_{001} and d_{002} steps, as observed on the (001) surfaces of $NiSO_4{\cdot}6H_2O$ crystals grown from an aqueous solution.

4.2. Spiral and two-dimensional nucleation growth

At low and intermediate supersaturations, most crystals grow *via* a spiral growth mechanism, which is induced by outcropping dislocations with a Burgers vector component perpendicular to the growth surface. The Burgers vector, **b**, of a *perfect* dislocation is equal to one or the sum of two or more unit translations in the crystal (Hull & Bacon, 1965). For example, in an I cell, these unit translations are $[\frac{1}{2}, \frac{1}{2}, \frac{1}{2}]$, [100], [010] and [001]. It can be shown that the component of $\mathbf{b} = [u, v, w]$ perpendicular to a face (hkl) has a length of $|hu + kv + lw|d_{hkl}$. This is the total step height emitted from a spiral dislocation. For a perfect dislocation ending on a face parallel to a plane $(hkl)_u$, $\mathbf{b}_\perp = |hu + kv + lw|d_{(hkl)_u}$, with $|hu + kv + lw|$ equal to zero or a positive integer, m. In this case, the total step height generated is $md_{(hkl)_u}$ for each turn of the spiral. If $m = 0$, no spiral growth occurs. In the nomenclature proposed by Frank (1981), a dislocation is described as 'rampant' if $m > 0$ and 'couchant' if $m = 0$. For low-index faces and unit-length Burgers vectors, m often equals one and the situation is as described in the previous sections. For larger m, the multiple spiral step generally splits into unit-height steps as a consequence of entropy repulsion at the dislocation outcrop, where the step spacing is extremely small (Maiwa *et al.*, 1998; DeYoreo *et al.*, 1994; Wang *et al.*, 1990; Cuppen *et al.*, 2000). In these cases, an m-fold spiral develops and (8) can again be used. The same pattern is obtained, except that the emission frequency, f, is about m times higher than for a single spiral.

For *partial dislocations*, $|hu + kv + lw|$ is generally not an integer, and in these cases the height of the spiral steps is not an integer times $d_{(hkl)_u}$. If a pair of partials, connected by a stacking fault, is sufficiently separated then isolated spirals develop, which do not generate the complete set of sublayers within $d_{(hkl)_u}$. This process leads to a lowering of symmetry. For instance, Aquilano *et al.* (2003) found that for partial dislocations with $\mathbf{b} = [001]/2$ ending on the (001) surface of α-amylase crystals, spiral growth resulted in a new polytype, the symmetry of which was lowered from $P2_12_12_1$ to $P2_1$. The 'partial' spiral did not generate the sequences of AB layers

that would be expected for a 2_1 axis perpendicular to the surface; only a stacking of *A* layers was formed.

If the new layers are formed by random two-dimensional nucleation growth, no concentric step patterns develop and the models developed in this paper cannot be applied. On the other hand, the criterion based on the systematic extinction of X-ray reflection can still be used to predict the symmetry-induced periodic change of two-dimensional nucleus orientation in successive growth layers, as was found for different proteins by Plomp *et al.* (2002).

4.3. Pseudosymmetry and pseudointerlacing

AFM topography of growth spirals on the (001) surfaces of $Ba(NO_3)_2$ crystals grown in an aqueous solution, which crystallize in space group $P2_13$, does not reveal step interlacing, despite the presence of a 2_1 axis perpendicular to the growth face (Maiwa *et al.*, 1998). However, in this case, the concentric step patterns, made up of half-unit-height steps, d_{200}, exhibit a twofold *pseudosymmetry*. With regard to the anisotropy in step velocity, this makes the adjacent growth slices (pseudo)-translation equivalent and no interlacing will occur. Another case of the absence of interlacing due to pseudosymmetry was observed and calculated for the growth of (0001) SiC-6*H* at higher temperatures (van der Hoek *et al.*, 1982). In this case, probably as a result of surface diffusion limited growth, the step velocity is isotropic and the step patterns emitted from the spiral centre become circular. This highest possible symmetry in step velocity makes the adjacent d_{002} slices (pseudo)translation equivalent and interlacing no longer occurs. From crystal growth theory, it is well known that smaller kink energies, higher temperatures and supersaturations or surface diffusion limited growth on a crystal surface with three-, four- or sixfold symmetry reduces the anisotropy of step velocity (Burton *et al.*, 1951; Sunagawa & Bennema, 1982; Swendsen *et al.*, 1976; van Enckevort, 1997). If in such cases the step velocity becomes more or less independent of step orientation then adjacent steps will not intersect and interlacing will be absent. Here growth proceeds by circular steps of subslice height.

Step interlacing has also been encountered in the region where two arrays of differently oriented macrosteps contact one another. Since here the splitting off and subsequent recombination of unit-height or multiple steps from the macrosteps is related neither to symmetry nor to the occurrence of subslices, this phenomenon will be denoted as *pseudointerlacing*. Pseudointerlacing, the principle of which is shown in Fig. 12, has for instance been observed for macrosteps on the (010) surface of KH-phthalate crystals (Fig. 8 of van Enckevort & Jetten, 1982) as well as on the (110) surfaces of garnet crystals by Zamozkij & Klevsov (1965). Macrosteps on a crystal surface develop if a perturbation in an equidistant step train emitted from a growth centre leads to an accumulation of steps. This situation occurs if, for two adjacent steps with reduced separation, the step behind moves faster and overtakes the one in front. Such an outcome is possible in those cases of surface diffusion limited growth, where the adsorbed growth units enter a step more easily from its rear side than from its front (Schwoebel, 1969). A similar instability of a step train also occurs if steps are retarded by time-dependent impurity adsorption on the crystal surface (van der Eerden & Muller-Krumbhaar, 1986; Kandel & Weeks, 1994, 1995; de Theije *et al.*, 2000). In both situations, the formation of macrosteps is a statistical process, which differs for adjacent arrays of differently oriented steps. Therefore, the terraces that belong to neighbouring macrostep arrays of different orientation have a different height. These height differences are compensated by a zigzag splitting off of lower steps from the macrosteps, as shown in Fig. 12. It is clear that this phenomenon of pseudointerlacing is related neither to symmetry nor to the occurrence of subslices with thickness less than $d_{(hkl)_u}$.

5. Conclusions

Observation of growth spirals and other concentric step patterns on *F*-type crystal surfaces with the help of optical microscopy and AFM often reveals a periodic splitting and recombination of unit-height steps into lower steps. Such interlacing of steps may occur if one unit slice, $d_{(hkl)_u}$ (the Miller indices *hkl* being corrected for the systematic extinctions of non-primitive lattices), consists of a sequential stacking of two or more connected subnets. Then a splitting of unit-height steps into substeps occurs if the identity of the slowest advancing substep changes with step orientation. If the adjacent subslices are not related by a translation combined with the action of a point-symmetry element perpendicular to the surface then the occurrence and the characteristics of this so-called *incidental interlacing* are not imposed by symmetry. *Symmetry-induced interlacing* occurs if, because of the presence of screw axes or glide planes perpendicular to the surface, the anisotropy of step propagation of the adjacent sublayers is related by symmetry, or alternatively if a plane (*hkl*) parallel to the *F* face exhibits a systematic extinction of X-ray reflection, which is not due to a non-primitive lattice. In these cases, apart from pseudo-symmetry, interlacing must occur. The precise details of the step interlacing and the

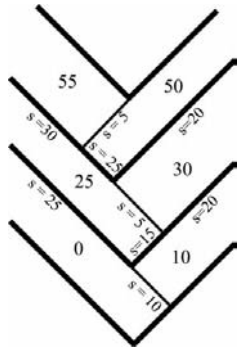

Figure 12
Pseudointerlacing; the height differences of the corresponding terraces in adjacent arrays of differently oriented macrosteps are compensated by a splitting off of lower steps from the macrosteps. Large numbers: terrace heights; numbers preceded by S: step heights.

trajectories of the split steps follow from a mathematical description of the step patterns as functions of space, time and symmetry. On some crystal surfaces, cross-laced macrosteps were reported; this phenomenon is described as *pseudo-interlacing*. It is not imposed by symmetry or by the presence of substeps but results from a compensation of the height difference of adjacent, differently oriented, macrosteps.

References

Aquilano, D., Veesler, S., Astier, J. P. & Pastero, L. (2003). *J. Cryst. Growth*, **247**, 541–550.

Bennema, P. (1965). *Z. Kristallogr.* **121**, 312–317.

Bennema, P. (1993). *Handbook of Crystal Growth*, Vol. 1a, *Fundamentals: Thermodynamics and Kinetics*, edited by D. T. J. Hurle, pp. 481–581. Amsterdam: Elsevier.

Bennema, P. (1996). *Sir Charles Frank, an Eightieth Birthday Tribute*, edited by R. G. Chambers, J. E. Enderby, A. Keller, A. R. Lang & J. W. Steeds, pp. 46–78. Bristol: Adam Hilger.

Bennema, P., Giess, E. A. & Weidenborner, J. E. (1983). *J. Cryst. Growth*, **62**, 41–60.

Bennema, P., Meekes, H., Boerrigter, S. X. M., Cuppen, H. M., Deij, M. A., van Eupen, J., Verwer, P. & Vlieg, E. (2003). Proceedings of the Sixth International Workshop on Crystal Growth of Organic Materials (*CGOM* 6), Glasgow, 17–21 August 2003. Review paper submitted to *Cryst. Growth Des.*

Burton, W. K., Cabrera, N. & Frank, F. C. (1951). *Philos. Trans. R. Soc. London Ser. A*, **243**, 299–358.

Cherepanova, T. A., Didrihsons, D. T., Bennema, P. & Tsukamoto, K. (1989). *Morphology and Growth Unit of Crystals*, edited by I. Sunagawa, pp. 163–199. Tokyo: Terra Scientific Publishing.

Cuppen, H. M., van Veenendaal, E., van Suchtelen, J., van Enckevort, W. J. P. & Vlieg, E. (2000). *J. Cryst. Growth*, **219**, 165–175.

Derksen, A. J., van Enckevort, W. J. P. & Couto, M. S. (1994). *J. Phys. D Appl. Phys.* **27**, 2580–2591.

De Yoreo, J., Land, T. A. & Dair, B. (1994). *Phys. Rev. Lett.* **73** 838–841.

Eerden, J. P. van der & Muller-Krumbhaar, H. (1986). *Electrochim. Acta*, **15**, 1007–1017.

Enckevort, W. J. P. van (1997). *Facets of 40 Years of Crystal Growth, a Tribute to Piet Bennema on the Occasion of his Retirement*, edited by W. J. P. van Enckevort, H. L. M. Meekes & J. W. M. van Kessel, pp. 51–70. University of Nijmegen, The Netherlands.

Enckevort, W. J. P. van, Janssen, G., Vollenberg, W., Schermer, J. J., Giling, L. J. & Seal, M. (1993). *Diamond Relat. Mater.* **2**, 997–1003.

Enckevort, W. J. P. van, Bennema, P. & van der Linden, W. H. (1981). *Z. Phys. Chem. Neue Folge*, **124**, 171–191.

Enckevort, W. J. P. van & Jetten, L. A. M. J. (1982). *J. Cryst. Growth*, **60**, 275–285.

Enckevort, W. J. P. van & Klapper, H. (1987). *J. Cryst. Growth*, **80**, 91–103.

Frank, F. C. (1951). *Philos. Mag.* **42**, 1014–1021.

Frank, F. C. (1981). *J. Cryst. Growth*, **51** 367–368.

Grimbergen, R. F. P., Bennema, P. & Meekes, H. (1999). *Acta Cryst.* A**55**, 84–94.

Grimbergen, R. F. P., Meekes, H., Bennema, P., Strom, C. S. & Vogels, L. J. P. (1998). *Acta Cryst.* A**54**, 491–500.

Hartman, P. (1969). *Growth of Crystals*, Vol. 7, edited by N. N. Sheftal, pp. 53–58. New York: Consultants Bureau.

Hartman, P. (1973). *Crystal Growth, an Introduction*, pp. 367–402. Amsterdam: North Holland.

Hartman, P. (1987). *Morphology of Crystals*, Vol. A, pp. 269–319. Tokyo: Terra Scientific Publishing.

Hartman, P. & Perdok, W. G. (1955*a*). *Acta Cryst.* **8**, 49–52.

Hartman, P. & Perdok, W. G. (1955*b*). *Acta Cryst.* **8**, 521–524.

Hartman, P. & Perdok, W. G. (1955*c*). *Acta Cryst.* **8**, 525–529.

Heide, G. & Follner, H. (1996). *Cryst. Res. Technol.* **31**, 171–177.

Heide, G., Follner, H., Jackson, R. A. & Wilde, P. J. (1996). *Cryst. Res. Technol.* **31**, 959–967.

Hoek, B. van der, van der Eerden, J. P. & Tsukamoto, K. (1982). *J. Cryst. Growth*, **58**, 543–553.

Hull, D. & Bacon, D. J. (1965). *Introduction to Dislocations. International Series on Materials Science and Technology*, Vol. 37. Oxford: Pergamon Press.

Kandel, D. & Weeks, J. D. (1994). *Phys. Rev. B*, **49**, 5554–5564.

Kandel, D. & Weeks, J. D. (1995). *Phys. Rev. B*, **52**, 2154–2164.

Li, T., Morris, K. R. & Park, K. (2000). *J. Phys. Chem. B*, **104**, 2019–2032.

Maiwa, K., Plomp, M., van Enckevort, W. J. P. & Bennema, P. (1998). *J. Cryst. Growth*, **186**, 214–223.

Meekes, H., Bennema, P. & Grimbergen, R. P. F. (1998). *Acta Cryst.* A**54**, 501–510.

Nowak, G., Pakula, K., Grzegory, I., Weyher, J. L. & Porowski, S. (1999). *Phys. Status Solidi*, **216**, 649–654.

Nye, J. F. (1984). *Physical Properties of Crystals: their Representation by Tensors and Matrices*, p. 20. Oxford: Clarendon Press.

O'Connor, B. H. & Dale, D. H. (1966). *Acta Cryst.* **21**, 705–709.

Plomp, M., van Enckevort, W. J. P. & Vlieg, E. (2000). *J. Cryst. Growth*, **216**, 413–443.

Plomp, M., McPherson, A. & Malkin, A. J. (2002). *J. Cryst. Growth*, **237–239**, 306–311.

Rijpkema, J. J. M., Knops, H. J. F., Bennema, P. & van der Eerden, J. P. (1983). *J. Cryst. Growth*, **61**, 295–306.

Schwoebel, R. L. (1969). *J. Appl. Phys.* **40**, 614–626.

Stoica, C., Meekes, H., Enckevort, W. J. P., Verwer, P., Vlieg, E., van Hoof, P. J. M. C. & Kasperen, F. M. (2004). In preparation.

Suchtelen, J. van (1995). *The Geometry of Crystal Growth: Morphology of Crystals*, Part C, edited by I. Sunagawa. Dordrecht: Kluwer Academic Publishers.

Sunagawa, I. & Bennema, P. (1979). *J. Cryst. Growth*, **46**, 451–457.

Sunagawa, I. & Bennema, P. (1982). *Preparation and Properties of Solid State Materials*, Vol. 7, edited by W. R. Wilcox. New York: Marcel Dekker.

Swendsen, R. H., Kortman, P. J., Landau, D. P. & Müller-Krumbhaar, H. (1976). *J. Cryst. Growth*, **35**, 73–78.

Theije, F. K. de, Schermer, J. J. & van Enckevort, W. J. P. (2000). *Diamond Relat. Mater.* **9**, 1439–1449.

Verheijen, M. A., Vogels, L. J. P. & Meekes, H. (1996). *J. Cryst. Growth*, **160**, 337–345.

Verma, A. R. (1951). *Philos. Mag.* **42**, 1005–1012.

Wang, X.-S., Goldberg, J. L., Bartelt, N. C., Einstein, T. L. & Williams, E. D. (1990). *Phys. Rev. Lett.* **65**, 2430–2433.

Zamozkij, V. D. & Klevsov, P. V. (1965). *Kristallografiya*, **10**, 668–676.

Zauner, A. R. A., Aret, E., van Enckevort, W. J. P., Weyher, J. L., Porowski, S. & Schermer, J. J. (2002). *J. Cryst. Growth*, **240**, 14–21.